TÉCNICO LISBOA

Instrumentation and testing of RPC (Resistive Plate Chamber) detectors in the Pierre Auger collaboration

Author: Pedro Alexandre Glória Cardoso

ABSTRACT: In this thesis it is going to be presented an overview of the physical characteristics of a certain particle detector: Resistive Plate Chambers (RPCs). This work was done as a part of the Muon Auger RPC for the Tank Array (MARTA) project which is an upgrade proposal to insert RPCs below the water tanks of the Pierre Auger observatory. This observatory is a pioneer in astroparticles experiments and has obtained various results and measurement of great interest in cosmic ray physics. These RPCs' primary objective is to detect and measure the muonic component of the particle shower started by a cosmic ray event.

We will focus in the understanding how the particle ionizes the gas and how the charge multiplication phenomenon occurs inside a chamber avalanche. With this knowledge we will give theoretical predictions of the induced signals and the RPC's efficiency.

We find that the experimental results are in line with what we predicted based on charge multiplication phenomenon. There was a big focus on measuring and understanding signals and charges/voltage spectra. We have measured the average charge of the first 6 ns of the avalanche signal to be around 8 pC. We have estimated the percentage of streamers in our acquisitions as being 2.4 %. There were also measurements of the efficiency of around 60 % or 80 % depending on the electronics acquisition setup.

Keywords: RPCs, project MARTA, observatory Pierre Auger, cosmic rays, particle detectors, charge spectra.

1. Introduction

What are cosmic rays? Cosmic rays are highly energetic particles that enter earth's atmosphere coming from the outer space. While it is still uncertain what their origins are, it is certain that they are a source of information of the whole universe around us. Nevertheless there have been indications that they might come from supernovas and other astronomical events, even though this is still highly controversial subject in the scientific community.

When a cosmic ray enters in contact with the atmosphere it scatters in the presence of other nuclei creating secondary particles. As the primary particle collides with an atmospheric nuclei, it will be produced as a result: pions (charges -1, 0,+1), eventually baryons (other protons and neutrons) and charged kaons. The neutral pions will give the main contribution to the electromagnetic cascade. Charged pions and kaons will be the main contributors for the creation of muons. In the end, the result of one highly energetic particle hitting the atmosphere is mainly an electromagnetic component (electrons, positrons and photons) and a muonic component. This can be explained by the lifetimes of the particles involved in an EAS, meaning that other particles are unstable and will most likely decay before reaching the ground level.

Nowadays, the Pierre Auger Observatory the world's largest is composed of both ground water Cherenkov detectors tanks [3] and fluorescence telescopes. The first ones are the ones disposed in array configuration, and they consist of large tanks filled with water. High energy particles crossing the water emit Cherenkov radiation, because they have velocities superior to light in this medium. Three PMT's (photomultipliers) tubes symmetrically distributed at a distance from the center of the tank detect this Cherenkov radiation. The fluorescence telescopes consist typically of large mirrors and segmented UV cameras and detect the light emitted from de-excitation of nitrogen molecules. This information is cross compared with the ground detections and it's possible to reconstruct the path of the shower and do the primary particle characterization with a very large number of samples.

Observatories exploit the cosmic ray energy spectrum by using very large areas in order to detect higher energy cosmic rays. Dealing with particles with energies between 10^{15} eV and 10^{20} eV, HECR (High Energy Cosmic Rays), is one of the main advantages of cosmic ray experiments over particle accelerators experiments that will only be capable of achieving

energies of 14×10^{12} eV with the 2014 upgrade of the LHC (Large Hadron Collider).

The Pierre Auger Observatory has provided precious knowledge about UHECR. The current data suggests that for high energies there could exist composition change or a change in hadronic interactions. It is now demanding to separate the muonic component from the electromagnetic one. As such it is necessary to measure the muonic distribution and the muonic profile. In the end, it is desired that the Pierre Auger Observatory is able to measure mean number of muons and its RMS arriving at the detectors as function of the shower energy. The MARTA project is one of the currently developing solutions to address the muonic component of the shower individually.

The strategy proposed by MARTA (Muon Auger RPC for the Tank Array) is to place RPC detectors below each water tank (Figure 1). As it has been described above, these Cherenkov detectors are able to absorb most of the electromagnetic component of the shower. The RPC detectors placed below them will mostly be hit by the shower's muons. More information about muons in air showers can be found in [12].

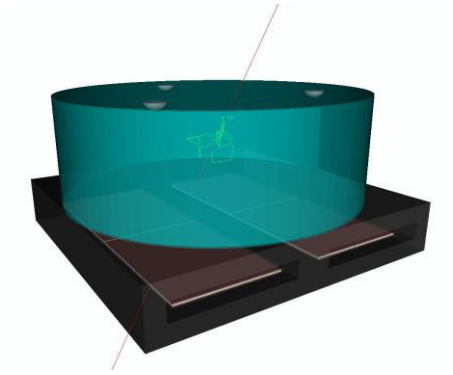

Figure 1 - RPCs inserted below Auger's water tanks.

This thesis is developed in the MARTA project context for the Pierre Auger Observatory and is developed in LIP-Lisbon. Its main purpose is to provide a detailed study of the characteristics and responses of an RPC unit detector prototype. There is also the objective to optimize and improve the hardware based on this information.

The prototype in study was constructed in LIP-Coimbra. It is a doublegap timing RPC with the objective of detecting muons and measuring their properties. Once it has been completely studied, test proofed and integrated with the correct electronics, its design will be replicated for the rest of the RPCs needed in the observatory.

2. Physics of RPCs

As particle detectors, RPCs can be included in a more general type of detectors: ionization chambers. Ionization chambers are gas filled chambers where incoming charged particles ionize the gas releasing electrons and forming ions. With an external electric field it is then possible to collect the charges in electrodes. Also ion-pairs can emerge from secondary ionizations giving rise to small clusters. This phenomenon can only occur if in a collision between the particle and the neutral molecule, the energy deposited is above 2 times the ionization potential, so that the ionized electron has enough energy to ionize a secondary molecule. As muons have big enough energies they are more likely to ionize the gas in small clusters rather than doing single ionizations as they cross the gas gap.

As it has been said before there is a need to introduce an electric field inside the chamber in order to collect the charges created within the chamber. If this field is relatively low the charges will drift to the electrodes, and the diffusion and recombination processes will be very prominent. However if there is a high electric field the charges will be much more accelerated towards the electrodes and there will be less tendency for those processes to occur.

Charges in their way to the electrodes are subject to many collisions with the gas molecules. As charges are more accelerated they will achieve bigger kinetic energies between collisions, to the point where this energy might exceed the ionization potential of the gas molecules. When this requirement is met there is a possibility that the charges collide with other neutral molecules and secondary ionizations might happen. Once again as the ions have greater masses they will achieve lower velocities in the same time than the electrons not contributing as much to the charge multiplication phenomenon. From the previous reasoning we may deduce that there will be a threshold for gases at which the electric field is big enough to accelerate electrons between collisions to energies above the ionization potential of the gas. This is related with the mean free path of the electrons in the gas but for most of the gases used in this kind of applications this threshold rounds 10 KV/cm.

The products of secondary ionization will also be subject to the high electric field and for that reason they will also have a chance of ionizing other neutral molecules. Consequently the charge multiplication will take shape of a cascade and will result in what is known as a Townsend avalanche. This process is easily described using a differential equation [19]:

$$\frac{dn}{n} = \alpha dx \qquad (1)$$

where n represents the number of electrons, dn the increment on the number of electrons, α is the Townsend coefficient and dx is the increment in length. For parallel detector structure α is a constant and so the solution for the equation will be theoretically an exponential as follows [19]:

$$n(x) = n_0 e^{\alpha x} \qquad (2)$$

where n_0 is the initial number of electrons and x is the distance from the initial position. The Townsend coefficient is then the physical constant that reflects how the charge multiplies inside the detector. This constant has a typical curve for different gas mixtures and varies with the electric field applied. There is an example on Figure 2 [22] of an experimentally measured curve (black dots) of the effective Townsend coefficient as function of the electric field in normalized by the number of particles in a cm^3 (for R134a it is $6.67 \times 10^{18}\ cm^{-3}$ at PTN). The normalized electric field is in Td ($1\ \mathrm{Td} = 10^{-17}\ \mathrm{V.cm^2}$).The effective Townsend coefficient is defined by the difference between the Townsend (α) and the attachment coefficient (η) that expresses the recombination rate inside the chamber.

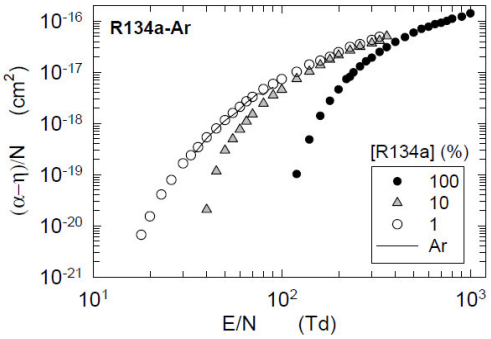

Figure 2 - Normalized effective Townsend coefficient as a function of the normalized electric field in Td for various R134-a mixtures [22].

In the early works on RPCs there was a discrepancy in the measured charges of an avalanche and the theoretical predictions. The issue was that for the Townsend coefficient that we have on RPCs and the high electric field applied it was expected that charges would be of the several orders of magnitude greater. This big difference of magnitude can be corrected if we account with the influence of the space charge effect. This effect is of the utmost importance on RPC electron avalanches. The space charge effect can be described as the phenomenon that happens when the number of charges on the avalanche reaches a point where it starts to create its own electric field that will be added to the applied electric field.

The electrons in the avalanche are accelerated by the electric field imposed. As the charges move they will induce a signal on the pickup electrodes (conductors) placed on top of the chamber. Because of the lower drift velocity ions will induce lower current values on the pickup electrodes. The signal induction process on a pad is not straightforward. In fact, we must consider that the avalanche is positioned where the weighting electric field lines are uniform in order to get a clean signal. That is also the reason why pads must have much bigger areas than the thickness of the RPC chamber. Another information that we can get from this figure is that pads can detect avalanches from another neighbor pad even though the correspondent induction is distorted.

We will now start to follow a simple model described in [24], to make a theoretical prediction of the signal induced. In this model we will take in consideration only the resulting electron charge from the avalanches inside the chamber, meaning we will not consider the ion impact on the signal. This can be considered a good approximation because this induced signal will take a few nanoseconds and the total signal that includes charges related to the ions movement will take typically a microsecond.

The current induced on the electrode as it has been described in [24] has the following theoretical expression:

$$I(t) = \frac{E_W}{V_w} e_0 v N(t) \qquad (3)$$

where $I(t)$ is the current induced in the instant t, E_W is the weighting field, is the electric field in the gas gap if we put the pickup electrode to the potential V_w and ground all others, e_0 is the electron charge, v is the electron drift velocity inside the gas, and $N(t)$ is the number of electrons arriving at the electrode at the instant t. In Figure 3 there is a measurement of the electron drift velocity for different gas mixtures [22].

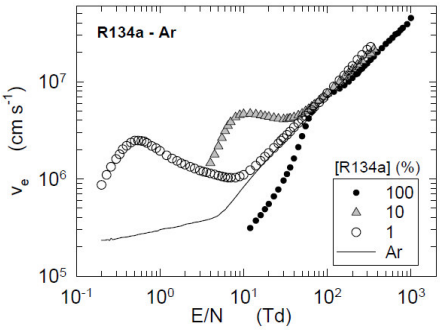

Figure 3 - Drift velocity as a function of the normalized Electric Fields for various R134-a mixtures [22].

In experimental setups the ratio between E_W and V_w must be calculated from the geometry of the RPC unit. For this we will assume an uniform E_W as the transversal dimension of the system is much larger than the width of the camera. In that case we can use the relations for a capacitor with n number of layers of permittivity ε_i, thickness d_i and infinite length:

$$\sum_{i=0}^{n} E_i d_i = V_w, \qquad \varepsilon_i E_i = \varepsilon_j E_j \tag{4}$$

where E_i is the electric field in layer i, and the second condition is true for adjacent layers. In order to calculate the electric field inside the chamber we will have to know the geometry of the detector. In Figure 4 we can see a schematic of the RPC unit used in this thesis.

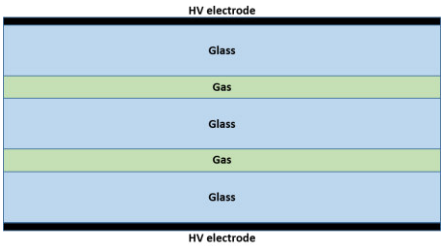

Figure 4 - RPC unit schematic.

For this geometry we can deduce the expression for the ratio between weighting field and weighting potential is as follows:

$$\frac{E_W}{V_w} = \frac{\varepsilon_r}{3g + 2d\varepsilon_r} \tag{5}$$

where ε_r the relative permittivity of glass, g is the thickness of the glass and d is the thickness of the gas gap. With $\varepsilon_r = 7.5$, this ratio can be calculated as can be calculated as $\sim 0.357\ mm^{-1}$.

The actual electric field across the chamber will be simply given by:

$$E = \frac{V}{d} \tag{6}$$

where E is the imposed electric field, V is the voltage in one of the electrodes (the other one is set to the symmetric value) and d is the thickness of the gas gap. With $V = 5.6\ KV$ and $d = 1\ mm$ we obtain an actual electric field of $\sim 56\ KV/cm$. From figures 2 and 3 (black dots on both figures) we can now estimate the effective Townsend coefficient $\sim 20.48\ mm^{-1}$ and the electron drift velocity $\sim 140\ \mu m/ns$.

As it has been stated before the avalanche grows like a smooth exponential and so does the charge. The current that may be induced in a single instant will also grow exponential from this reasoning.

With the understanding of the physical processes the amplitude can be estimated. First of all the signal will be produced by more than one clusters with probably more than one electron. To estimate the number of clusters N_0 we can just divide the chamber length by the means free path for that gas. Typical mean free path for the mainstream gases in RPCs is $\sim 0.1mm$ and in our case we have two $1mm$ chambers so we expect the number of clusters per incoming particle to be around 20 statistically speaking. The typical average number of electrons n_{av} per cluster is around 2.7 for similar setups. We will assume that this clusters will be distributed evenly throughout the gas gaps.

Hence, if we had very big time resolution, it would be expected theoretically that the signal induced would be a sum of arriving separate clusters' avalanches, with small discontinuities. In fact it is observed a smooth transition between clusters' signals and for that reason it is more relevant to have an enveloping function. This enveloping function has been described in the model used [24] as the following expression:

$$N_{env}(t) = N_0 n_{av} \left(1 - \frac{tv}{d}\right) e^{(\alpha-\eta)vt} \times \Theta\left(\frac{d}{v} - t\right) \tag{7}$$

where the notation has been kept from before and $N_{env}(t)$ is the number of electrons in the avalanche at instant t, and $\Theta(x)$ is a step function with which the previous expression is multiplied. This function serves as an indication of when electrons reach the glass at which point the avalanche will stop and the number of electrons quickly goes to 0. The term $\left(1 - \frac{tv}{d}\right)$ expresses the stage of the avalanche. This expression will be later used in the calculation of the current induced. This formula depends on the average of various physical constants meaning that this will also result in an average typical signal. Situations that may result in variations of signal between events are: more/less clusters than the average expected, more/less electrons per cluster than the average, all clusters very close/far from the pickup electrodes (as opposing to evenly distributed). Computing the parameters of our RPC chamber into this equation we will get the following development of the number of electrons inside the avalanche shown in Figure 5.

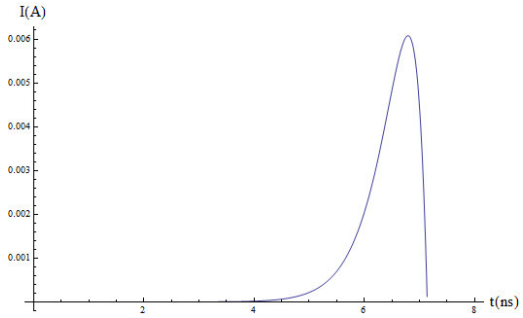

Figure 5 - Theoretical estimation of the induced signal from one of the gas chambers.

The signal predicted develops in a short time and does not take into account the readout system. The systems used to acquire these signals have a bandwidth that makes it impossible to output perfectly the signal. Moreover, the system capacitances introduce a relaxation time on the signal. So a fast rise is expected, corresponding to the calculated signal followed by a tail corresponding to the relaxation of the system. Nevertheless, there are some approximations in this model such as not considering the space charge effect which will lead us to an overestimation of the amplitude. If we integrate this signal over ~8 ns we will get the charge induced of ~5.786 pC which is of the same order of magnitude of what is measured in laboratory.

The efficiency of a RPC chamber is intrinsically related to its capability to induce the charge created in the gas gap on the pickup electrodes. What this means is that not all the charge created inside the chamber will be detected on the electronics. Hence, to have an efficient event one cluster must produce an avalanche that is not reattached/recombined and stays above the charge threshold that is intrinsic to the experimental setup. It is also possible that one avalanche from one cluster has not enough charge to stay above threshold but the sum of all the avalanches from all the clusters reaches the threshold. This is not usually the case, because most of the times there is at least one avalanche that reaches the threshold (provided that this is not unrealistically high), and so in the model below this situation will not be taken in account. Overall we can conclude that the efficiency of a RPC will be the ratio of efficient events as described above over the total number of events.

In order to make some predictions of the efficiency of our particular setup it was followed a model that is fully described in [24]. For this thesis we will just use the final result deduced in the paper for the expression of the efficiency, that is as follows:

$$\varepsilon = 1 - e^{-(1-\frac{\eta}{\alpha})d/\lambda}\left[1 + \frac{V_W}{E_w}\frac{\alpha-\eta}{e_0}Q_t\right]^{1/\alpha\lambda} \quad (8)$$

where Q_t is the charge threshold, ε is the efficiency and the rest of the notation has been kept from the previous chapter. The efficiency will then actively depend not only on $\alpha - \eta$ but also on α and η explicitly. Also it will depend heavily on the charge threshold imposed.

Multi-gap systems have an improved performance over single-gap systems in terms of efficiency for the same gas gap width and Townsend coefficient. This effect has been studied to behave as follows [24]:

$$\varepsilon_n = 1 - (1 - \varepsilon_s)^n \quad (9)$$

where ε_n is the efficiency of a RPC with n gaps and ε_s is the efficiency of a single gap system in the same conditions. For our double-gap system the efficiency can than be recalculated as it is in Figure 6. As it was predicted the efficiency was greatly improved for the same parameters used before. Setting the values of the threshold to 250 fC and the Townsend coefficient to 20.48 mm^{-1} this model predicts an efficiency of ~0.88.

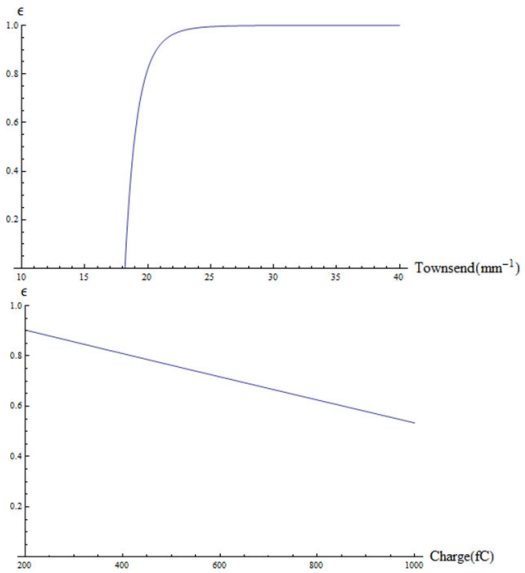

Figure 6 - The efficiency prediction for our double-gap system as a function of the Townsend coefficient (above) and as a function of the charge threshold (bottom).

3. RPC experimental tests

3.1. Oscilloscope and amplifier stage tests

In Figure 7 it is shown a sample acquisition with this setup. The voltage recorded by the oscilloscope (after amplification) is plotted against the time in

nanoseconds. It can be seen that the signal is detected ~150 ns earlier than the trigger meaning that there is a bigger delay on the trigger in this setup in comparison with the signal. The pulse is approximately ~10 ns wide and has an amplitude of ~120 mV. This signal shows a fast rise that is correspondent to the avalanche development and corresponds to the pulse calculated in chapter 2. However it has a large tail that corresponds to the relaxation of the signal through the discharge of the capacitances involved in this setup. Note that in this particular acquisition there are noticeable reflections in the signal cables providing two extra peaks in our signal. These reflections are mainly due to the impedance mismatch of the amplifier. Although the line has a characteristic impedance of 50Ω and it is terminated with a 50Ω resistor on the oscilloscope and that the amplifier is rated to 50Ω impedance, its impedance varies with the frequency of the signal.

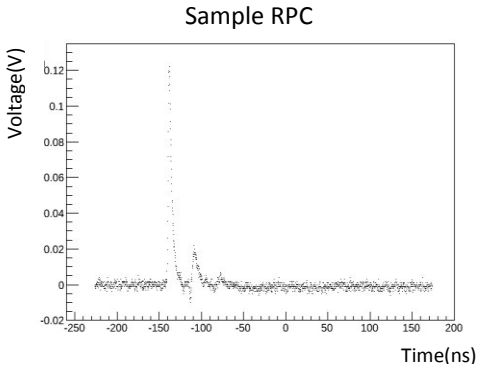

Figure 7 - Acquired typical signal with this setup.

For the purposes of this study it is now important to take a statistical look at the events of the RPC. For this reason it is required to have many events in the same set of conditions so that we can describe more accurately the behavior of the RPC unit. In Figure 8, we have an acquisition of 8339 events, correspondent to around 3 days with the used thresholds for the triggers of the scintillators. These acquisitions were done with $\Delta V = 11200V$. All the events are overlapped so we can see the tendency of the signal. We can see that the big majority of events are pulses around $\sim -130\ ns$ and there are very prominent reflections of the signals $\sim -100\ ns$ and $\sim -80\ ns$. This issue is caused by not properly terminating the transmission signals and it is a common situation in this kind of acquisition but can be avoided.

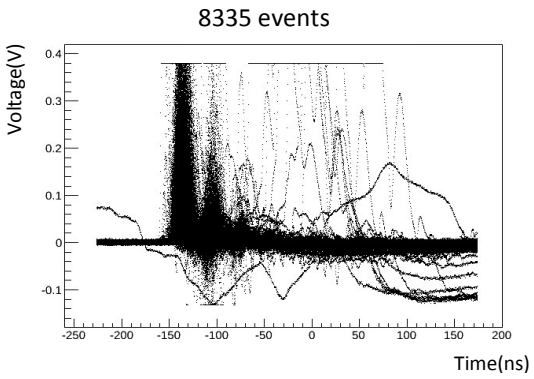

Figure 8 - Superposition of 8335 RPC events.

There are some "strange" events that were caused by erroneous triggers due to either electromagnetic interference inside room where the RPC was operated or simply because of two triggers with very small time interval between them. Also we can see many signals saturating the oscilloscope scale causing a horizontal line on the top. Since the oscilloscope is limited in the vertical resolution preference was given to the observation of small amplitude signals, saturating some of the signals, mainly streamers. As we are operating the RPC in avalanche mode, streamers are undesirable. Streamer probability is however closely related to the RPC working parameters and "health" and as such an estimation of the fraction of streamers is interesting. Most of the rising and falling edges outside the higher density part of this superposition will be caused by these streamers events which are demanding for the RPC and their signals tend to be more inconsistent regarding their shapes.

The resulting charge spectrum from the 8335 events acquisition can be observed in Figure 9. This plot is presented with a logarithmic vertical scale for easier visualization of the spectrum and bins with a lower number of entries. This is a typical measured charge spectrum for our setup. We can see primarily a peak at very small charge, representing inefficient events. For such events there was a coincidence trigger from the scintillators but the RPC response had no charge. However pronounced, only ~10% of the events are represented in this region. After the non-efficient peak, the spectra shows a hump and then decreases almost exponentially. This peak is associated with the most probable value for the charge and is very useful for the characterization of the RPC working condition. The position of this peak will vary with the HV, temperature and gas conditions inside the chamber. Also there is a slight deviation from the exponential fall around 15 of charge that corresponds to streamers. This deviation usually corresponds to a more prominent peak than what we observe on this case. The streamer peak can be used to compare between two acquisitions

if they were likely done in the same conditions. In fact if we consider that the streamer mean charge peak is always located in the same place it could be used to rescale the spectra. Moreover, if two RPCs are working in the same conditions then this peak can be used to cross-calibrate the two spectra.

As an addition, a gamma distribution was fitted to the charge spectrum on Figure 9. There were also other distributions that could have been used like the Weibull and the LogNormal, but the final choice was to use the Gamma due to its versatility and to the fact that it was already implemented on the ROOT software. The fitted gamma distribution in Figure 9 has the following expression:

$$f(x) = 455.171e^{-0.6869x}(-0.8884 + x)^{1.43891} \quad (10)$$

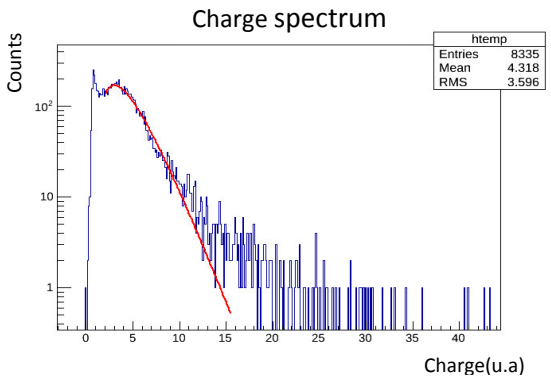

Figure 9 - Charge spectrum of the 8335 events acquisition integrated over the full window of the oscilloscope.

3.2. Calibration tests

The need to quantify absolutely our setup lead us to undergo some calibration tests. For this purpose it was needed an electrically equivalent of an RPC to replace it in the circuit. The focus of the calibration was on the charge spectra because it is the most important and comparable information to other related studies. As such we would want a basically source that gave us similar shaped current/voltage peak which we would know exactly the charge. It was chosen to use the scheme showed in Figure 10, because it was the simple and cheap approach to the problem.

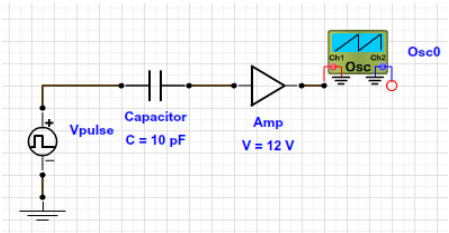

Figure 10 - Calibration circuit.

Using the time constant in our advantage we will use the pulse corresponding to the rising edge of the input in the most similar way possible to the RPC pulse. The falling edge is disregarded completely. The square wave is generated with a large period to allow for a full charge and full discharge in between edges. It can be seen that it is still an approximation (in terms of shape) but if we know exactly what charge our calibration pulse holds it should be possible to extrapolate that information to use in the RPC pulse. The charge in a capacitor is expressed by:

$$Q = CV \quad (11)$$

where Q is the charge, C the capacitance and V the voltage applied across the capacitor. If the exponential has a big enough slope and the frequency of the input signal is low enough the voltage across the capacitor can be approximated by the input high level, for the rising edge.

This will lead us to obtain a multiplying constant for our arbitrary units of about ~7.821 pC. Using this constant of calibration and reintegrating only the first 6 ns of each event's pulse it was obtained the charge spectrum in pC in Figure 11. As it can be observed the new charge spectrum peak is around ~8 pC. This result is of the same order of magnitude as the predicted in the last chapter. There is still a very big peak for the noise associated with this acquisition around ~0 pC. Above 35 pC there is a rise over the exponentially decreasing number of events tendency due to streamer events but overall this acquisition does not appear to have a high percentage of streamers. The gamma distribution fitted as the following expression:

$$f(x) = 16.577e^{-0.26535\,x}(1.52819 + x)^{2.14821} \quad (12)$$

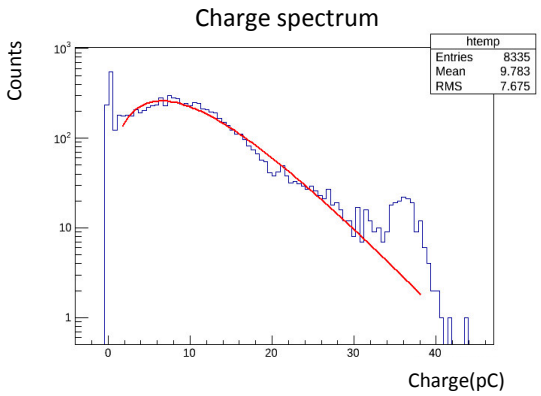

Figure 11 - The charge spectrum in pC of the first 6 ns of each signal for the 8335 event acquisition with logarithmic scale and a gamma distribution fit.

With this logarithmic scale we can see clearly the streamer peak at around ~ 38 pC. As it has been stated before it is usual for acquisitions to have one peak for the noise one broader peak for the avalanche signal and one peak for the streamer signal. In Figure 11 it is now very clear those three peaks as well as their charges in pC for our RPC unit. By summing all the events in bins above ~ 35 pC we obtain that there are a percentage of streamers of about ~2.4%.

3.3. MARTA-PREC acquisitions

MARTA Prototype Readout Electronics Classic version (MARTA-PREC) is a proposed readout discrete electronic setup to acquire all pads of the RPCs used in MARTA project. In Figure 12 we can see a scheme of this PREC acquisition setup.

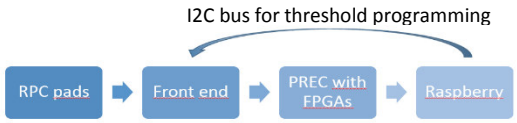

Figure 12 - Scheme of the PREC acquisition setup.

The first acquisitions done with this setup were background tests on the pads. For these acquisitions it was changed the software on the Raspberry Pi to iterate the thresholds on the front end board in steps of 10 mV. The FPGAs were also programmed to count in a standardized time interval what the number of events detected above the threshold were – this was called background rate. In Figure 13 it can be seen the result of such an acquisition for the b1 pad with the background rate as a function of the threshold voltage. As this is an acquisition by thresholds the results are going to be a complementary cumulative version of the voltage spectrum and for that reason not directly comparable with the spectra obtained with the method discussed in 3.1. From this complementary cumulative nature we can expect that for every bin the number of events will be exponentially lower, and for that reason we may assume a negative exponential for the trend. Hence it was fitted an exponential curve to the data which has the equation shown in the figure.

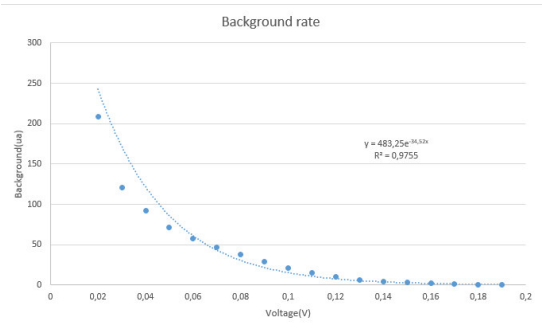

Figure 13 - Cumulative background spectra of pad b1.

As this acquisition takes the form of a complementary cumulative distribution (or survival function), then by statistical definition, in order to obtain the original spectrum we need to obtain the signal symmetric of the derivative of this plot. Hence, if we are able to differentiate this set of points we will be able to compare this new results with the oscilloscope results. This was accomplished to do by calculating the slope of the line that connects any two consecutive points in these data (this is an approximation of a derivative) with the following expression:

$$m_n = \frac{B_n - B_{n+1}}{V_{n+1} - V_n} \qquad (13)$$

where m_n is the value that will be used as the derivative for point n, B_n is the background rate for point n and V_n is the voltage threshold for the point n. The results can be seen in Figure 14 side by side with a background acquisition on the same pad. It can be seen that because of the 10 mV steps the PREC acquisition results do not have as much resolution as the oscilloscope results. Nevertheless it can be seen a straightforward equivalency between the two voltage/amplitude spectra.

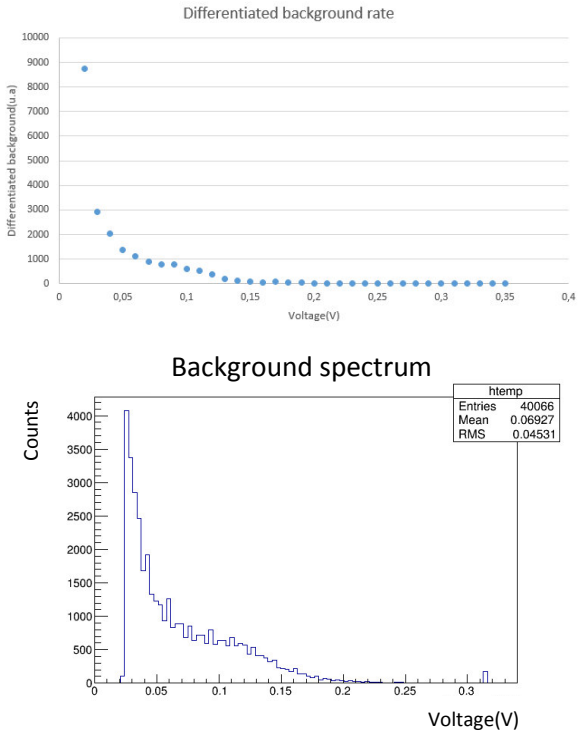

Figure 14 - Background spectra acquisitions done by the PREC setup (above) and by the 3.2.1 setup (bottom).

After the background checks for uniformity amongst pads we proceeded to multiple pad triggered acquisitions. For these procedures we have selected the

8 nearest pads to the input of gas in the chamber to make sure we have healthier spectra possible. Then we choose the first threshold value for the acquisition of 35 mV. We let the electronics acquire for 1 day and then we had to choose a higher threshold and wait for another day. The graph obtained in Figure 15 took several days to make because each point would correspond to 1 day of acquisition. Because of this big acquisition time it was impossible to insure that every acquisition would have the same number of points. For this reason it was decided to use in the vertical scale the ratio between the number of detections and the total number of coincidence triggers, which is basically a normalization of the number of detections. This was the only way to make each point comparable with all the others but might lead to statistical variation errors due to the fact that there are acquisitions with more events than others. Also as one of the scintillators used is a narrow object it could only insure the passage of a charged particle through one of the pads. Hence, it was considered a detection when there was a trigger and the b1 pad signal was above the threshold. Nevertheless all the statistic from the other pads can be later used to verify the cross-talk.

These ratios between detections/events can also be interpreted as a measurement of the efficiency of the RPC. As it was predicted in chapter 2 the efficiency will depend on the charge threshold that in this case takes the form of a voltage threshold. Once again this is reasonable assumption in a relative analysis of the spectrum because the two variables are assumed to be correlated. We see that for ~35 mV of threshold, which is a value safely above the noise, the RPC reaches an efficiency of 83.5% for the oscilloscope measurements and 61.8% for the PREC measurements. This is in line with the prediction of 82.2% even though it was for a 250 fC charge threshold and we cannot compare directly this value with the voltage threshold used.

As a final approach to this data we can also take a look at the 8 pad information rather than focusing only on the central one. In Figure 15 we can see a comparison between the acquisitions with an output of 1 in pad b1 (blue) and acquisitions with an output of 1 on any pad of the 8 set (red). As it was predictable the second one includes the first for that reason its number of detections will always be superior. What is interesting to notice is that on average there is only a small percentage of particles (around 5%) that do not actually trigger the pad b1 when there is a coincidence trigger even though they have are detected in a neighbor pad. This gives a better insight on the triggering mechanism and also provides and extra degree of validity to previous results. There is also another set of points (grey) that represent the situations when the pad b1 triggers but there are one or more of the other pads that also trigger. Of the total number of detections on the b1 pad (blue) on average there is a ~26% of them that also trigger other pads. This can be due to one of two reasons: either there was cross-talk or the PREC system logic levels sometimes erroneously change.

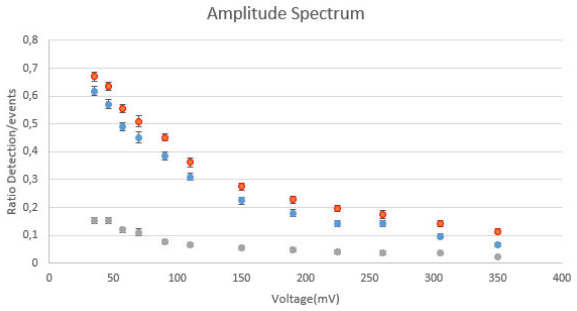

Figure 15 - Complementary cumulative voltage spectrum comparison between acquisitions triggering pad b1 (blue) and triggering at least one pad of 8 chosen (red). With the color grey there are the points that trigger b1 but also trigger other pads.

4. Conclusions

The MARTA project was able to successfully demonstrate the possibility to use low gas flow RPCs and operate them in harsh environment. Currently six detectors are installed in the Pierre Auger site:

- 2 RPCs are being used in a telescope setup for the calibration of an Auger tank (Gianni Navarra).

- 2 RPCs are installed below a water tank, inside a concrete structure, in the field (Argentine pampa). They are located on top of each other in order to make efficiency tests. Monitoring results are showing a smooth operation at low gas flow.

- 2 RPCs are being tested indoors with the MAROC prototype electronics solution.

Until now, all the RPCs being tested have shown good performances. Nevertheless as the acquisition electronics are in a prototype phase, they can still be unstable. It is expected however to stabilize its operation in the near future and to upgrade the DAQ to the MAROC solution.

RPCs have proven to work efficiently as trigger detectors. They are one cheap and reliable solution that can be applied to most particle counting experiments. With the in-depth study of the characteristics of the RPCs it was possible to develop and optimize electronics that would suit its readout and acquisition.

This thesis provided an overview over the theoretical predictions of signals, charges and efficiencies, as well as test measurements results of the same signals,

spectra, charge, efficiency, background tests. The experimental data appears to be in line with the theoretical predictions even though there are some approximations and cheap approaches on both sides.

REFERENCES

[1] M. V. S. R. a. B. V. Sreekantan, “Extensive Air Showers,” World Scientific, 1999.

[2] P. Grieder, Extensive Air Showers - High Energy Phenomena and Astrophysical Aspects, Springer, 2010.

[3] P. Bauleo, “A water tank Cherenkov detector for very high-energy astroparticles,” Nuclear Instruments and Methods in Physics Research A, vol. 406, 1998.

[4] “Pierre Auger Observatory Website,” [Online]. Available: www.auger.org.

[5] I. Allekotte, “The Surface Detector System of the Pierre Auger Observatory,” arXiv:0712.2832 [astro-ph], 2007.

[6] J. Lozano-Bahilo, “Results of the Pierre Auger Observatory on High Energy Cosmic Rays,” em Journal of Physics: Conference Series 160, 2009.

[7] P. Abreu, “Measurement of the proton-air cross-section at √s=57TeV with the Pierre Auger Observatory,” arXiv:1208.1520v2 [hep-ex], 2012.

[8] K. Greisen, “End to the Cosmic-Ray Spectrum?,” Phys. Rev. Lett., vol. 16, 1966.

[9] G. T. Z. a. V. A. Kuz'min, “Upper Limit of the Spectrum of Cosmic Rays,” Soviet Journal of Experimental and Theoretical Physics Letters, vol. 4, 1966.

[10] C. M. a. N. Scharf, “HEAT - a low energy enhancement of the Pierre Auger Observatory,” arXiv:1106.1329 [astro-ph.IM], 2011.

[11] A. Etchegoyen, “AMIGA, Auger Muons and Infill for the Ground Array,” arXiv:0710.1646 [astro-ph], 2007.

[12] L. Cazon, “A model for the transport of muons in extensive air showers,” Astroparticle Physics, vol. 36, 2012.

[13] C. Lippmann, “Detector Physics of Resistive Plate Chambers,” PHD Dissertation by Johann Wolfgang Goethe-Universitat Frankfurt, 2003.

[14] P. Eiras, “Software development and Performance Analysis of the HADES Resistive Plate Chamber Time-of-Flight Detector at GSI,” PHD Dissertation by Universidade de Santiago de Compostela, 2011.

[15] V. Ammosov, “The HARP resistive plate chambers: Characteristics and physics performance,” Nucl. Instr. and Meth. A, vol. 578, p. 119, 2007.

[16] A. N. Akindinov, “Study of gas mixtures and ageing of the multigap resistive plate chamber used for the Alice TOF,” Nucl. Instr. and Meth. A, vol. 533, p. 93, 2004.

[17] W. Yi, “Study on the performance of multi-gap resistive plate chambers,” Nucl. Instr. and Meth. A, vol. 538, p. 425, 2005.

[18] A. Shuettauf., “The Front-End Electronics for the HADES RPC Wall (ESTRELA-FEE),” Nucl. Phys. B (Proc. Suppl.), vol. 158, p. 47, 2006.

[19] G. F. Knoll, Radiation Detection and Measurement, Wiley, 2000.

[20] C. L. Werner Riegler, “The physics of Resistive Plate Chambers,” Nuclear Instruments and Methods in Physics Research A, vol. 518, p. 86, 2004.

[21] W. R. Leo, Techniques for Nuclear and Particle Physics Experiments, Springer-Verlag, 1993.

[22] E. Basurto, “Time-resolved measurement of electron swarm coefficients in tetrafluoroethane (R134a),” em 28th ICPIG, Prague, 2007.

[23] W. R. Christian Lippmann, “Space charge effects in Resistive Plate Chambers,” Nuclear Instruments and Methods in Physics Research A, vol. 517, p. 54, 2004.

[24] C. L. R. V. Werner Riegler, “Detector physics and simulation of resistive plate chambers,” Nuclear Instruments and Methods in Physics Research A, vol. 500, p. 144, 2003.

[25] C. Lu, “Induced Signal in RPC,” em SNIC Symposium, Stanford, 2006.

[26] P. Fonte, “Analytical calculation of the charge spectrum generated by ionizing particles in Resistive Plate Chambers at low gas gain,” Journal of Instrumentation, 2013.

[27] p. c. L. Lopes.

[28] M. Paterno, “Calculating Efficiencies and Their Uncertainties,” 2003.

[29] L. Lopes, “Study of RPCs for autonomous fiels stations in cosmic ray research (Preliminary version),” Proceedings of science, 2014.